Available online at www.sciencedirect.com
SCIENCE DIRECT®
Separation and Purification Technology 43 (2005) 245–255
Separation Purification Technology
www.elsevier.com/locate/seppur

Air gap membrane distillation 2. Model validation and hollow fibre module performance analysis

C.M. Guijt[a,*], G.W. Meindersma[b], T. Reith[b], A.B. de Haan[b]

[a] *Friesland Coberco Dairy Foods, P.O. Box 87, 7400 AB Deventer, The Netherlands*
[b] *University of Twente, Faculty of Science and Technology, Separation Technology Group, P.O. Box 217, 7500 AE Enschede, The Netherlands*

Received 21 April 2004; received in revised form 5 August 2004; accepted 17 September 2004

Abstract

In this paper the experimental results of counter current flow air gap membrane distillation experiments are presented and compared with predictive model calculations. Measurements were carried out with a cylindrical test module containing a single hollow fibre membrane in the centre and a well-defined air gap situated around the fibre. The experimental results show that the previous developed predictive model, with membrane parameters determined from gas permeation experiments, describes correctly the dependence of water vapour flux on temperature level, temperature difference, air gap total pressure, hot water flow and membrane type. At atmospheric air gap pressure, the measured fluxes per saturated water vapour pressure difference between the bulk flows (0.08–0.10 kg/m^{2}h mbar) are comparable with those presented in literature. A reduction of the total air gap pressure to the saturated water vapour pressure of the hot water feed flow temperature of 65 °C, raises the flux by a factor of three. Next to the water vapour flux, the energy efficiency of the process is very important. The measured energy efficiencies (typically 85–90% for a 3 mm air gap and a hot water feed temperature of 65 °C) are slightly below the theoretical values (95–98%), which could be explained by a small heat loss to the surroundings. For air gaps of 1.5 mm or smaller, the energy efficiency is reduced to less than 70%, due to thermal conduction across product water bridges between the membrane fibre and the condenser surface. An optimal air gap is about 3 mm wide and has a total pressure that is equal to or slightly below the saturated water vapour pressure of the hot water entering the hollow fibre membrane.

Keywords: Air gap membrane distillation; Experiments; Energy efficiency; Module design; Desalination

1. Introduction

For desalination of water three different membrane distillation configurations are used. In all cases saline feed water is brought into contact with a hydrophobic micro-porous membrane through which water vapour can diffuse and by which liquid water is retained. In direct contact membrane distillation (DCMD) fresh water with a lower temperature than the saline feed water is in direct contact with the membrane at the permeate side [1–4]. Desalination takes place as water vapour diffuses across the membrane as a result of the water vapour pressure difference. A drawback of this configuration is the heat loss due to heat conduction across the membrane. Air gap membrane distillation (AGMD) uses a cold condenser wall placed at a short distance from the membrane at the permeate side [1,5–7]. The air gap functions as a thermal insulation between membrane and condenser wall. However, it is also an extra resistance towards mass transfer, so that AGMD generally results in lower fluxes than DCMD. Finally, in vacuum membrane distillation (VMD) the permeate space is evacuated and the water vapour is condensed outside the membrane module [8,9]. This results in higher fluxes, but higher value energy is needed to keep the permeate space evacuated.

The technique that is the subject of this study is based on AGMD (see Fig. 1). Cold seawater feed flows through a condenser tube with non-permeable hydrophilic walls via a

* Corresponding author. Tel.: +31 570 695 946; fax: +31 570 695 918.
E-mail address: cm.guijt@fcdf.nl (C.M. Guijt).

1383-5866/$ – see front matter © 2004 Elsevier B.V. All rights reserved.
doi:10.1016/j.seppur.2004.09.016

Nomenclature

A_{module}	outer module surface between cold water entrance and exit (m^2)
Cp_{wl}	heat capacity of liquid water (J/kg K)
d_{ag}	air gap thickness (m)
E	energy efficiency as defined by Eq. (2) (%)
E_{evap}	latent heat of evaporation of product flow (J)
ΔE_c	energy change of the cold water flow during a membrane distillation experiment (W)
$\Delta E_{c,corr}$	energy change of the cold water flow corrected for heat loss to the surroundings (W)
$\Delta E_{c,no\ \Delta T}$	energy change of the cold water flow in case of no temperature difference between hot and cold water flow, energy loss (W)
ΔH_{vap}	average heat of evaporation (J/kg)
J	water vapour flux with respect to outer membrane radius (kg/m^2s)
L	effective fibre length (m)
m	mass flow rate (kg/s)
$p_w^0(T)$	saturated water vapour pressure of temperature T (Pa)
P_{ag}	air gap total pressure (Pa)
Δp_w	saturated water vapour pressure difference between hot and cold water bulk temperatures (Pa)
r_2	outer membrane radius at membrane–air gap interface (m)
r_3	outer air gap radius at air gap–product water interface (m)
r_4	condenser radius at product water–condenser interface (m)
R	relative resistance towards water vapour transport
Re	Reynolds number
T	temperature (°C)
ΔT	temperature difference between hot and cold water flow (°C)

Subscripts

av	averaged over module length
bottom	at module bottom
c	cold water flow
h	hot water flow
in	at flow entrance
top	at module top

heater into a micro-porous hydrophobic hollow fibre membrane in counter current mode. In this way the heat of evaporation from the vapour leaving the membrane is recovered like in multi stage flash evaporation. The tubes are separated by a gap from which non-condensable gases can be (partly) removed. This results in the advantageous energetic

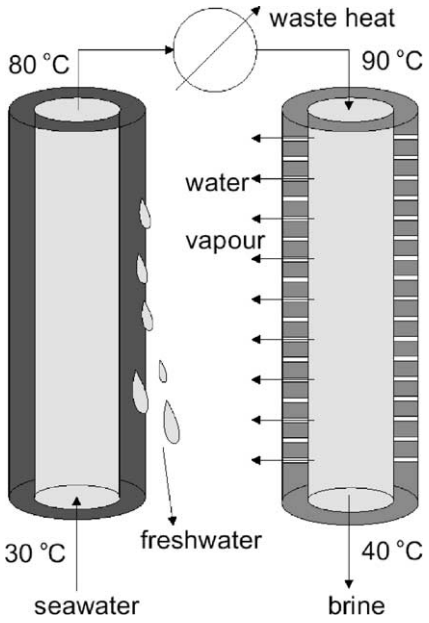

Fig. 1. Schematic presentation of AGMD in counter current flow configuration.

efficiency of AGMD while minimising the drawback of the extra resistance to mass transfer of the air gap. Although almost all AGMD studies have been carried out with flat sheet membranes [1,6,10–16], hollow fibres were preferred in this study. Hollow fibre modules have a simpler construction, while the heat transfer coefficient inside hollow fibre membranes is comparable to that of flat sheet membranes with well-designed spacers [17,18].

The objective of this study is to formulate criteria for maximum water vapour flux and energy efficiency of a process according to Fig. 1, since these are the two most important indicators for module performance in desalination by membrane distillation. Depending on air gap width, membrane type, and operating temperature, calculations claim theoretical energy efficiencies between 70% and 99% for AGMD [6,12,20]. This means that 70 to 99% of the energy drop of the hot water flow is used for evaporation of water and that 1–30% is lost by heat conduction across the membrane and the air gap. Compared to DCMD, AGMD should be considerably more energy efficient, especially at lower temperatures. For constant temperature difference between the hot and cold water flow, reducing the temperature level results in a lower saturated water vapour pressure difference between the hot and the cold water flow Δp_w. Since this water vapour pressure difference is the driving force for vapour transport, the vapour flux decreases at decreasing temperature. For constant temperature difference the heat conduction remains the same, resulting in lower energy efficiency at lower temperatures. This negative effect is stronger for DCMD, because the conductive heat flow is relatively larger. Although the high potential energy efficiency of AGMD is often mentioned, little attention has been paid to measuring energy efficiencies in experiments so far. The only study known to us is of Kubota

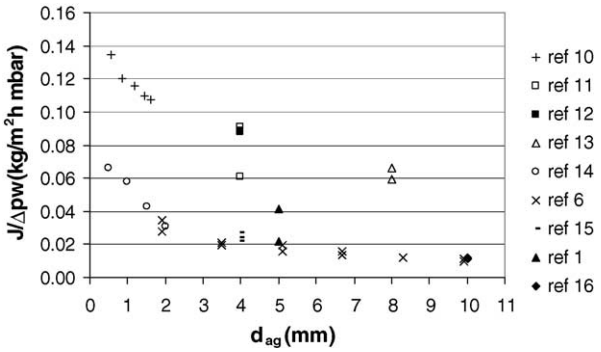

Fig. 2. Fluxes per water vapour pressure difference of bulk flows as a function of air gap width at atmospheric pressure for flat sheet membranes obtained from literature.

et al. who measured energy efficiencies of below 50% [5], which is much lower than expected.

As mentioned earlier, the major drawback of the air gap is that it gives an extra resistance to mass transfer, which can for example result in eight times lower fluxes for a 5 mm air gap compared to DCMD under similar circumstances [1]. Fig. 2 provides a literature overview of fluxes obtained so far in flat sheet AGMD. The vertical axis shows the flux in (kg/m^{2}h) divided by the driving force Δp_w in (mbar). Globally two lines, for different modules, can be distinguished between which the flux per driving force differs by a factor of 4 for large air gaps, which decreases to a difference of a factor of 2 for small air gaps. The results clearly demonstrate that the fluxes increase considerably by decreasing the air gap width. Jönsson et al. calculated that the optimal air gap width is 0.2 mm, resulting in large water vapour flux and low energy loss [20]. However, the practical value of this air gap width has never been tested and one can imagine that the condensed water vapour has not enough space in a 0.2 mm air gap.

Next to reduction of the air gap width, reducing the air gap pressure is another method to increase vapour flux. Fane et al. suggested removal of air from the membrane pores in DCMD in order to increase the water vapour flux [21]. Gostoli and Sarti showed that decreasing the air gap pressure from 1000 to 400 mbar increased the flux with a factor 2.4 [16]. However, since they carried out their measurements with a 10 mm air gap (see Fig. 2) the flux remained relatively low.

The process and module parameters influencing water vapour flux and energy efficiency are the temperature difference between hot and cold water flow, water temperature level, water flow velocities, air gap pressure, air gap width, and membrane type. In a previous paper [19] we have presented a predictive model that has been developed to evaluate the influence of those parameters on the module performance for the process shown in Fig. 1. In the present study that model is validated with experiments. The obtained experimental results, supported by interpretation according to the model, are used as the basis for the formulation of module optimisation criteria with respect to water vapour flux and energy efficiency.

2. Experimental methods

2.1. Experimental set-up

In order to obtain a well defined air gap, modules were used containing only one single hollow fibre membrane positioned in the centre of the concentric annulus for the cold water flow. As a consequence the membrane areas used in the present study are relatively small: 3.5–8.3 cm^2 for fibres with a length of 29.5 cm, while in similar studies reported in literature for flat sheet membranes, areas of 19–520 cm^2 [6,10–16] and even 1.9–2.9 m^2 [5] were used. This small membrane area results in low mass and energy flows, which make additional demands on the accuracy of measuring instruments and controls in the experimental set-up.

The experimental set-up is schematically depicted in Fig. 3. The demineralised water in the hot and cold feed tanks was thermostated with a Julabo F32 thermostat bath, which maintained a constant temperature within 0.04 °C in the feed tanks. The circulation pumps for both water flows were Verdergear 1000 digit gear-wheel pumps with a micropump model 186–000 pump head, which was able to generate low mass flows, down to 0.3 kg/h, with negligible pulsation.

The hot water flow, ranging from 0.3 to 1.4 kg/h, was pumped from the feed tank to the module top where it entered the hollow fibre membrane. The hot water mass flow was measured after the bottom exit of the module by an Elite CMF010M coriolis flow meter with an error between 0.4 and 1% and returned to the hot water feed tank. The cold water flow, ranging from 1 to 20 kg/h, was pumped from the feed tank to the bottom of the module where it entered the concentric annulus around the membrane fibre. The cold water mass flow was measured after the top exit of the module by a Brooks flowmate LSN40 with an error of around 2% and returned to the cold water feed tank.

Insulation of the feed channels proved insufficient for controlling the temperatures of the flows at the module entrances. Therefore, two heating wires were mounted along the flow channels from feed tank to module, enabling regulation of the entrance temperature of the water flows within 0.3 °C. The temperatures at all module entrances and exits were measured with 4-wire pt100's. After calibration their mutual deviation was less than 0.03 °C. The flow temperatures were measured as close to the module as possible, as shown in Fig. 4. The measurement signals of all temperature sensors and both flow meters were collected with a Keithley 2700 multimeter and stored by a pc at 1 min intervals.

The product water, which condensed on the inner wall of the concentric annulus around the membrane fibre, was collected in a measurement cylinder below the membrane module of which the level was read every 10–15 min. By conducting steady state experiments at least for one hour,

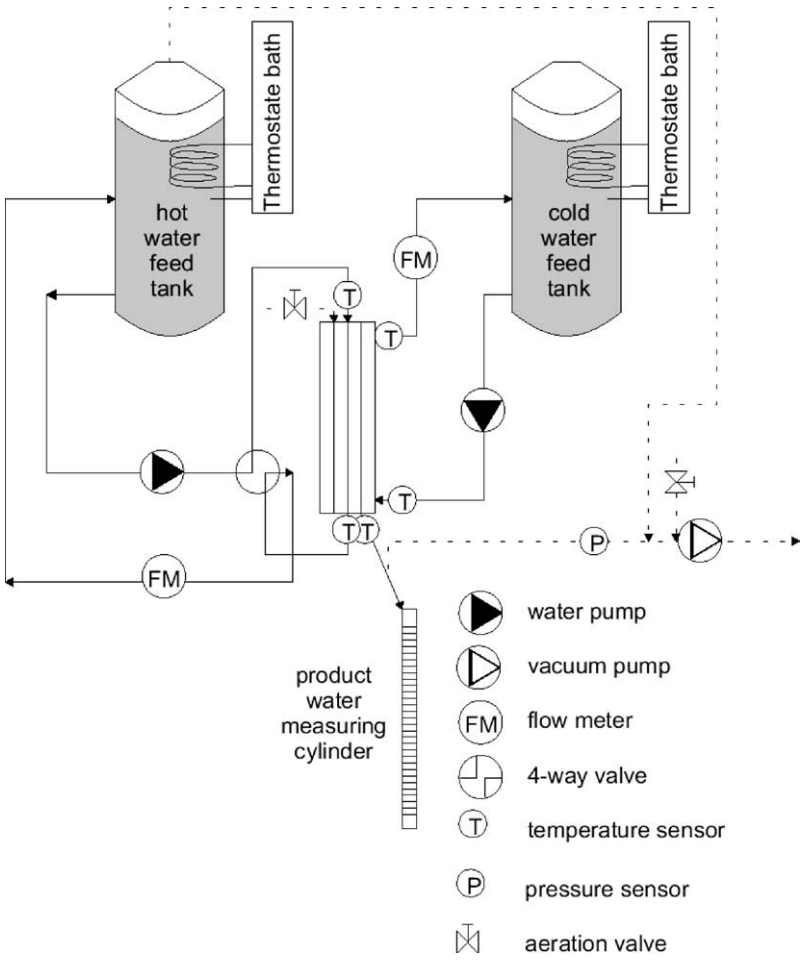

Fig. 3. Counter current flow AGMD setup.

the average value of the product flow, ranging from 2.5 to 12 ml/h, could be measured with an error of 1–4%.

The module air gap and the hot water feed tank were evacuated with a Vacuubrand MZ C2 membrane vacuum pump. Because the module was not completely air tight, the vacuum pump had to remain turned on during operation to maintain a constant pressure. The aeration valve on the pump was used to regulate the vacuum pressure. The vacuum pressure was measured with an Ebro vacumeter VM1500 that has an error of 0.4% at atmospheric pressure increasing to 1.3% at 100 mbar. By evacuating the air gap via the product water outlet, the vacuum pump helped the product water flowing down thus preventing product water accumulation in the module. Although not strictly necessary, the hot feed water tank was also evacuated in order to reduce the possibility of membrane wetting induced by pressure differences across the membrane.

2.2. Modules and membranes

Fig. 4 shows some details of the membrane distillation module. The module body was made of stainless steel, which is a convenient construction material because of its high thermal conductivity, hydrophilic behaviour and resistance to corrosion in demineralised water. Polyoxymethylene (POM) connection parts holding the membrane were screwed in the module body. These plastic parts formed a heat conduction barrier between the hot and the cold water flow. The hollow fibre membrane was fixed precisely in the middle of the air gap by gluing it in the connection parts with polyurethane resin (PUR). To prevent evaporation in the module top and bottom, the first and last two centimetre of the fibre were covered with PUR. The effective fibre length for evaporation was, therefore, 29.5 cm. At the module bottom, the free space between the connection part and the product water outlet was filled with PUR so that the product water could not accumulate there. A cotton thread was placed with one end in the bottom of the module and the other end in the top of the product water measurement cylinder in order to facilitate the product water flow across several connections on its way down.

For the measurements four modules were used, which differ only in diameter. By using modules with different diameters the air gap width, which is the inner condenser surface radius minus the outer membrane fibre radius, is varied. Values for the inner condenser surface radius (r_4) of all modules are listed in Table 1. The membrane fibres used are two polyethy-

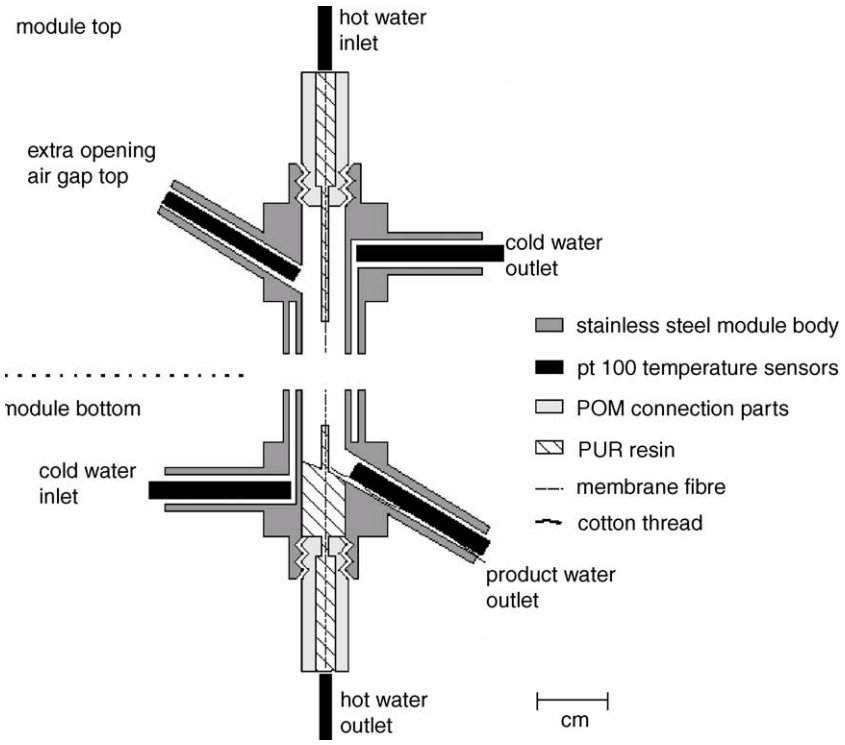

Fig. 4. Details of configuration for top and bottom of the module with condenser radius (r_4) of 3 mm.

Table 1
Air gap widths in (mm) for studied combinations of module and membrane fibre

Module $r_4/10^{-3}$ (m)	3.00	2.00	1.00	0.75
Membrane fibre				
PE VA12	2.73	1.73	0.73	0.48
PE FA16	2.81	–	–	–
UPE test	2.55	–	–	–

lene fibres of Mitsubishi: EHF540VA-12 and EHF270FA-16, abbreviated to PE VA12 and PE FA16 in this paper, and one ultra high density polyethylene test fibre of Millipore, called UPE test. The most important properties of these fibres are listed in Table 2 , while more detailed mass transport properties have been presented in a previous paper [19]. The resulting air gaps for the studied combinations of membrane type and module are listed in Table 1. Pieces of membrane fibre could only be used once in a module, because removal of the fibre from the module led to the destruction of the fibre. The piece of fibre used in a particular experiment is indicated by the number behind the fibre name.

Table 2
Membrane properties

Membrane fibre	Outer radius/ (10^{-6} (m))	Wall thickness/ (10^{-6} (m))	Porosity	Average pore size/(10^{-6} (m))
PE VA12	270	90	0.77	0.18
PE FA16	190	55	0.70	0.21
UPE test	450	250	0.57	0.26

2.3. Measurement conditions

Table 3 shows an overview of the experiments carried out. The temperature difference between hot and cold water flow at the module top (ΔT_{top}) was varied between 3 and 15 °C, with 10 °C as reference value when temperatures were not varied. The entrance temperature ranges of the hot and cold water flow ($T_{h,in}$ and $T_{c,in}$) were 40–70 °C and 30–60 °C, respectively, with 65 and 55 °C as reference values. The mass flow rate of the hot water flow (m_h) was varied between 0.6 and 1.3 kg/h. The air gap pressure (P_{ag}) ranged from the saturated water vapour pressure of the hot water flow (250 mbar for $T_{h,in}$ equals 65 °C) to atmospheric pressure, with 50 mbar above the saturated water vapour pressure of the hot water flow at the membrane fibre entrance as reference pressure. The membrane types and air gap widths (d_{ag}) used are listed in Table 1, the largest module (r_4 = 3.00 mm) and fibre type PE VA12 were chosen as references.

No measurements were carried out at different cold water flow rates, because the modules used are unsuitable for measuring its influence. Since the condenser surface is relatively large, the cold water has a relatively small resistance to heat transfer. Changing the cold water flow over the maximal range, could give a water vapour flux variation of at most 7% [22]. The reference cold water mass flow rate (m_c) was 20 kg/h, which is relatively high. As a consequence of that the cold water flow changed only slightly in temperature, about 0.2 °C, and functioned as additional module heat insulation.

Table 3
Overview of measurement conditions

Series		Module (r_4 (mm))	Membrane	$T_{h,in}$ (°C)	$T_{c,in}$ (°C)	m_h (kg/h)	$Re_{h,av}$	m_c (kg/h)	P_{ag} (mbar)
No.	Variable								
A	ΔT_{top}	3.00	PE VA12-6	65	50–62	1.3 (T)	2900	20	300
B	T_h, T_c	3.00	PE VA12-11	40–70	30–60	1.0 (L)	1400–2000	20	120–370
C	m_h	3.00	PE VA12-6	65	55	0.6-1.3	1200–2900	20	300
D1	P_{ag}	3.00	PE VA12-6	65	55	1.3 (T)	2900	20	250–1000
D2	P_{ag}	3.00	PE VA12-11	65	55	0.9 (L)	2000	20	250–1000
E	Membr.	3.00	PE VA12-6,-11	65	55	0.9 (L)	2000	20	300
			UPE test	65	55	1.0 (L)	2000	20	300
			PE FA16	55	45	0.4 (L)	1000	20	210
F	d_{ag}	0.75–3.00	PE VA125x	65	55	1.0 (L)	2000	0.9	300

L: laminar flow; T: turbulent flow.

3. Results and discussion

All calculation results presented in this section were obtained by simulations with the model presented in [19] carried out with gPROMS, a software product from Process Systems Enterprise Ltd. Within this tool all model equations are solved simultaneously, so there is no need for manual iteration procedures. For each calculation, values at the module top for the hot water mass flow and temperature, the cold water temperature, and the product water mass flow (=0) and temperature (just an estimated value to get the program running) were entered. Furthermore, total air gap pressure, and membrane and module properties had to be defined in each case.

3.1. Temperature influence on module performance

The results for the variable temperature difference and the variable temperature level series are given in Figs. 5–7. Fig. 5 shows the measured and calculated average water vapour flux as a function of the average driving force $\Delta p_{w,av}$, the logarithmic mean of the difference in saturated water vapour pressure p_w^0 of the bulk temperatures of the hot and cold water flow T_h and T_c at the module top and the module bottom:

$$\Delta p_{w,av} = \frac{[p_w^0(T_{h,top}) - p_w^0(T_{c,top})] - [p_w^0(T_{h,bottom}) - p_w^0(T_{c,bottom})]}{\ln(p_w^0(T_{h,top}) - p_w^0(T_{c,top})/p_w^0(T_{h,bottom}) - p_w^0(T_{c,bottom}))} \quad (1)$$

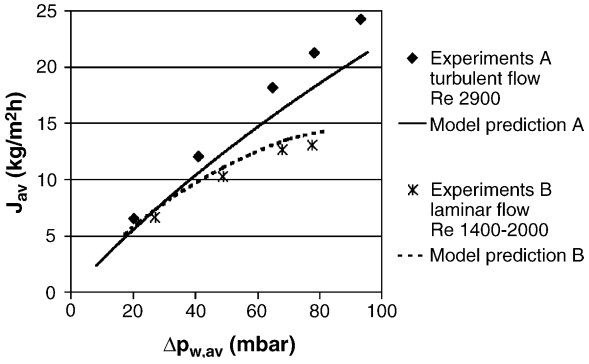

Fig. 5. Measured and predicted fluxes at variable driving force, series A ($T_{h,in}$ = 65 °C, ΔT_{top} = 3–15 °C, P_{ag} = 300 mbar), series B ($T_{h,in}$ = 30–70 °C, ΔT_{top} = 10 °C, $P_{ag} = p_w^0(T_{h,in}) + 50$ mbar).

Because the temperature of the hot water flow decreases with 2–6 °C, and the cold water flow remains almost at the same temperature, the driving force changes along the module. Calculations show that the logarithmic mean of the module top and module bottom driving force equals the overall mean driving force along the module. The average driving force $\Delta p_{w,av}$ increases with increasing temperature difference (series A), and also with increasing temperature level and constant temperature difference (series B), because the saturated water vapour pressure increases exponentially with temperature. The trends of flux increase with increasing driving force are predicted well by the model in both cases. The reason why for series A the flux increases much steeper at high driving force compared to series B is that series A was carried out with turbulent flow and series B with laminar flow, as is further explained in the next sub-section. Furthermore, in series A the model predicts a 13% lower flux than measured throughout the entire range, while in series B the predicted flux is 8% higher than measured, the cause of which will be discussed in Section 3.4.

The energy efficiency E is (%), shown in Figs. 6 and 7, is defined as the percentage of the decrease in energy content of the hot water flow that is used for evaporation, see Eq. (2).

$$E = \frac{J_{av} 2\pi r_2 L \Delta H_{vap}}{m_h(T_{h,in} - T_{h,out}) C p_{wl}} 100\% \quad (2)$$

In this equation J_{av} is the average flux with respect to the outer membrane surface in (kg/m^{2}s), r_2 the outer membrane radius in (m), L the effective membrane length in (m), ΔH_{vap} the heat of evaporation for the average hot water temperature in (J/kg), m_h the hot water mass flow in (kg/s), $T_{h,in}$ and $T_{h,out}$ are the hot water temperatures at the membrane entrance and exit in (K), and Cp_{wl} the liquid water heat capacity in (J/kg K). Fig. 6 shows the measured and calculated energy efficiency at various temperature differences

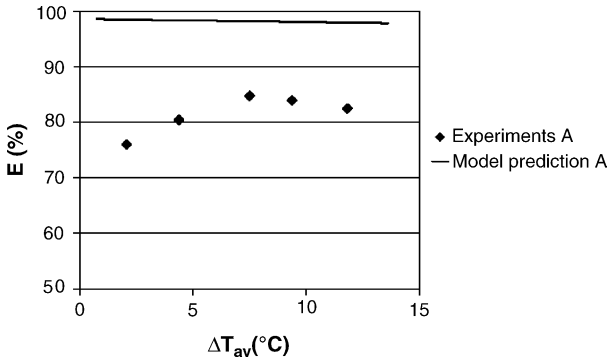

Fig. 6. Measured and predicted energy efficiency at variable temperature difference, series A ($T_{h,in}$ = 65 °C, ΔT_{top} = 3–15 °C, P_{ag} = 300 mbar).

and constant hot water temperature of 65 °C (series A). The measured energy efficiencies are below the theoretical ones, which can be explained by heat losses to the surroundings [22]. Because the current module design leads to low mass and energy flows, the heat loss to the surroundings is relatively large, despite of thorough thermal insulation. It is expected that higher efficiencies, approaching the theoretical ones, can be reached with larger modules. The lower measured energy efficiency for temperature differences below 5 °C can be explained by the lower resulting water vapour flux, so that the heat loss to the surroundings is relatively more important. For higher fluxes the energy efficiency is around 84%, which is much higher than the 50% measured by Kubota et al. [5]. Fig. 7 shows that the energy efficiencies obtained at various temperature levels (series B) are around 89%, which is high. The predicted energy efficiency decreases with decreasing temperature level as explained in the introduction. This trend cannot be observed for the measurements, which can be largely explained by the fact that heat loss to the surroundings at 40 °C is far less than at 70 °C. The reduced heat loss to the surroundings at lower temperature has a positive effect on the measured energy efficiency.

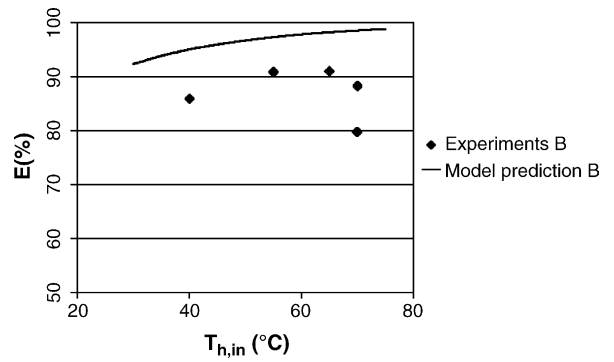

Fig. 7. Measured and predicted energy efficiency at variable temperature level, series B ($T_{h,in}$ = 30–70 °C, ΔT_{top} = 10 °C, $P_{ag} = p_w^0(T_{h,in}) + 50$ mbar).

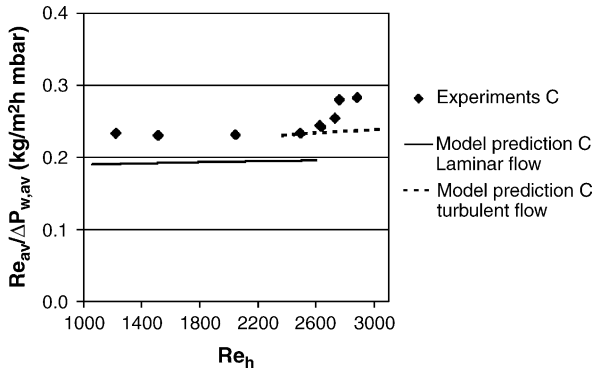

Fig. 8. Measured and calculated flux per driving force with variable hot water flow, series C (T_h = 65 °C, ΔT_{top} = 10 °C, P_{ag} = 300 mbar).

3.2. Influence of hot water mass flow rate on module performance

Fig. 8 shows the average flux per average driving force as function of the hot water flow Reynolds number (series C). Like in series A the predicted values are about 15% lower than measured, which will be discussed in Section 3.4. Around Reynolds equals 2750, a change from laminar to turbulent flow can be observed. Model calculations show that the enhanced heat transport in the hot water flow channel due to turbulent flow, results in a 20% larger effective temperature difference (the temperature difference across membrane and air gap). The same increase is measured for the water vapour flux per driving force. This flux increase is in line with measurements of Banat and Simandl [6,15] who observed flux increases of 10–20% between Re 2500 and Re 3000. The energy efficiencies of our measurement series C range from 85 to 95%.

3.3. Influence of air gap pressure on module performance

In Fig. 9 the observed fluxes per driving force for variable air gap pressure are presented. The flux (with respect to

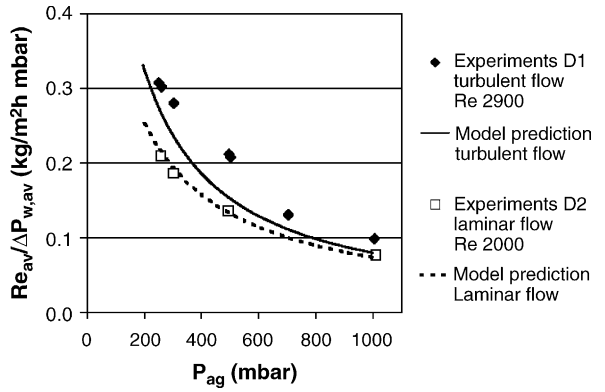

Fig. 9. Measured and calculated flux per driving force at variable air gap total pressure, series D1 and D2 ($T_{h,in}$ = 65 °C, ΔT_{top} = 10 °C, P_{ag} = 250–1000 mbar).

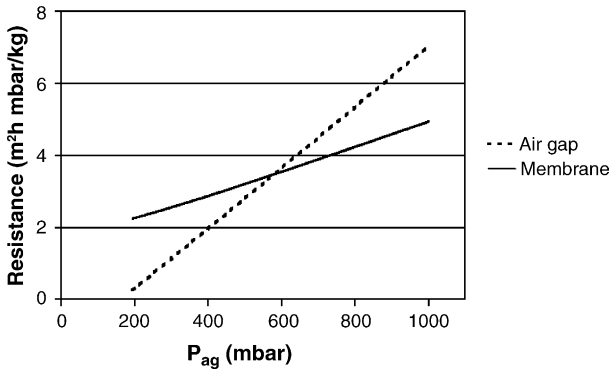

Fig. 10. Calculated resistance to mass transfer of membrane ($(p_{w,1}-p_{w,2})_{av}/J_{av}$) and air gap ($(p_{w,2}-p_{w,3})_{av}/J_{av}$) as a function of air gap total pressure, for measurement series D1.

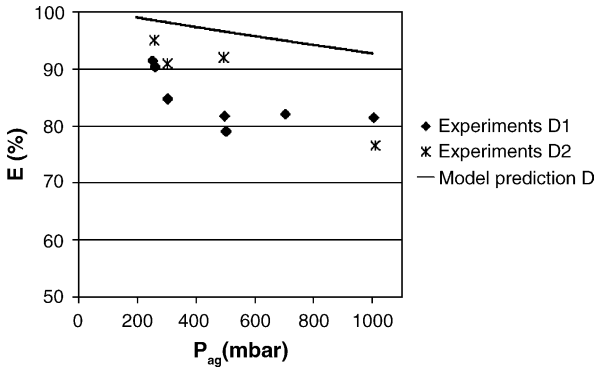

Fig. 11. Measured and predicted energy efficiency at variable air gap pressure, series D1 and D2 ($T_{h,in}$ = 65 °C, ΔT_{top} = 10 °C, P_{ag} = 250–1000 mbar).

the outer membrane surface) per driving force at atmospheric pressure is around 0.1 kg/m^{2}h mbar. For a comparison with the fluxes presented in Fig. 2, the cylindrical shape of the air gap must be taken into account. Although the cylindrical air gap is rather large in this experiment (r_3–r_2 = 2.73 mm), a flat air gap with the same resistance to mass transfer is only 0.7 mm ($r_2 \ln(r_3/r_2)$). This means that the obtained fluxes at atmospheric pressure are in line with the fluxes earlier presented in literature [10,14]. Reducing the air gap pressure from 1000 to 370 mbar gives a flux increase by a factor of 2.1 for laminar flow and a factor of 2.5 for turbulent flow, which is comparable with the increased fluxes found by Gostoli and Sarti [16]. Reduction of the air gap pressure to the saturated water vapour pressure of the hot water flow entering the module (250 mbar in Fig. 9) gives a flux increase by a factor of 2.5–3 compared to atmospheric pressure. It is concluded that the flux dependency on air gap pressure is predicted correctly by the model.

An important conclusion that can be made on basis of model predictions is that the air gap total pressure can be lowered beneath the saturated water vapour pressure of the hot water flow without boiling of the hot water flow. Calculations show that for a (turbulent) hot water flow of 65 °C, which has a water vapour saturation pressure of 250 mbar, there is still some air present at the hot water surface if the air gap total pressure is 200 mbar. This is due to a total pressure difference across the membrane at lower pressures. When the air gap pressure is reduced by 50 mbar, an additional increase in flux per driving force of almost 20% is calculated. However, the experimental set-up did not allow experimental confirmation of this flux increase, because the feed tank and the module were evacuated by the same vacuum pump.

Furthermore, the model can calculate the dependence of the resistance to water vapour transport on the total air gap pressure for the membrane ($(p_{w,1}-p_{w,2})_{av}/J_{av}$) and the air gap ($(p_{w,2}-p_{w,3})_{av}/J_{av}$) separately, see Fig. 10. At pressures below 200 mbar almost no air is present in the membrane and the air gap, and the membrane matrix is the most important resistance to mass transfer. With increasing pressure both air gap and membrane resistance increases linearly, as expected. The air gap resistance increase is steeper, because the air gap is thicker than the membrane. The ratio of the effective thickness of air gap and membrane, $\ln(r_3/r_2)$:$K_1\ln(r_2/r_1)$, with K_1 the molecular diffusion membrane morphology parameter [19], is 2.4, which equals the ratio of the slopes of the lines in Fig. 10.

Fig. 11 shows the obtained energy efficiencies at various air gap pressures. The theoretical efficiency is reduced with increasing air gap pressure, because of a reduction in water vapour flux and an increase in conductive heat loss, since air is a better heat conductor than water vapour. The measured efficiencies, although quite scattered, show a tendency to decrease with increasing pressure even more than expected. This is the result of heat losses to the surroundings, which become relatively more important at lower water vapour fluxes.

3.4. Membrane influence on module performance

For membranes PE VA12 and UPE test the standard entrance temperatures of 65 °C for the hot water flow and 55 °C for the cold water flow were used. However, for the PE FA16 fibre 10 °C lower temperature levels were used, because in this fibre hot water mass flow rates tends to decrease for temperatures above 55 °C, probably due to swelling of the PUR resin. Since the PE FA16 fibre is very thin it generates a relatively large pressure drop. In order to measure with an acceptable hot water flow, it was decided to measure at lower temperature levels.

The comparison between experimental and model results for different membranes is shown in Fig. 12. The model shows a very good agreement with PE VA12-11, UPE test and PE FA16, with deviations between −7.5 and +4.3%. This proves that the model parameters obtained with N_2 and CO_2 permeation experiments are suitable for predictive modelling of membrane distillation, and that the interaction of water vapour with the membrane is not much different from that of N_2 and CO_2. Of course the first conclusion only holds provided that the membrane fibres are sufficiently homogeneous (in length direction), which was demonstrated for the fibres of this study with the gas permeation experimental results [19].

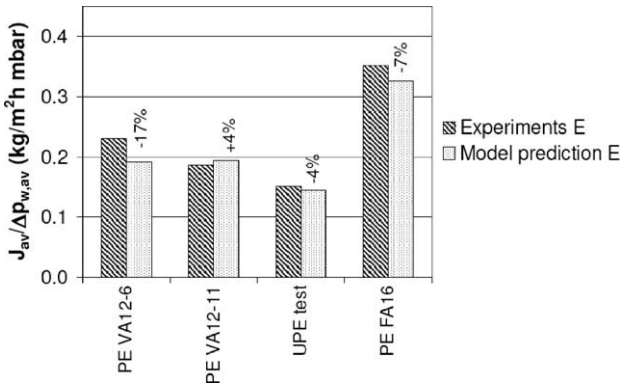

Fig. 12. Measured and calculated flux per driving force for different membrane fibres, series E ($T_{h,in}$ = 55–65 °C, ΔT_{top} = 10 °C, $P_{ag} = p^0_w(T_{h,in}) +$ 50 mbar). PE VA12-6 and PE VA12-11 are different pieces of the same PE VA12 fibre.

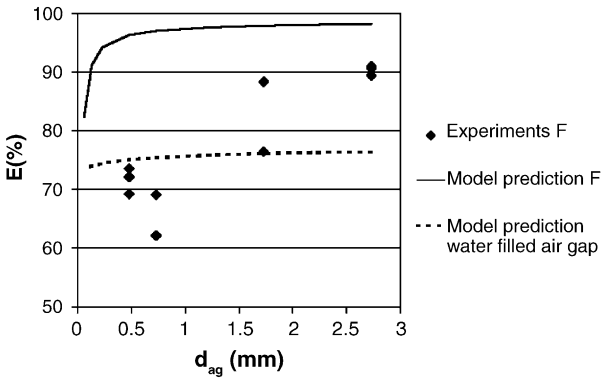

Fig. 14. Energy efficiencies obtained with experiments and model calculations, series F ($T_{h,in}$ = 65 °C, ΔT_{top} = 10 °C, P_{ag} = 300 mbar).

The reason for the relatively large deviation of PE VA12–6 (the piece of PE VA12 fibre that was also used in experiments A, C, D1 and F) is not very clear, but could be caused by operation at unacceptably high temperatures (above 70 °C) during start-up experiments.

From Fig. 12 it is clear that the PE FA16 fibre gives by far the largest water vapour flux and that UPE test generates the smallest flux per driving force. This is largely due to the fact that PE FA16 is a very thin membrane (55 μm, see Table 2), while UPE test, although it has a more permeable structure [19], is relatively thick (200 μm). PE VA12 has a similar structure as PE FA16, but a lower flux because of the larger wall thickness of 90 μm. However, the drawback of the PE FA16 fibre is the small inner diameter 270 μm, compared to 360 and 400 μm for PE VA12 and UPE test. This is why PE FA16 is not necessarily the most suitable fibre for the process, because of a larger risk of fibre blockage and higher pumping costs. The obtained energy efficiencies were in the range of 90–96%.

3.5. *Influence of air gap width on module performance*

The average fluxes per average driving force for variable air gap obtained in this study are shown in Fig. 13. The air gap is defined as the inner condenser surface radius (r_4) minus the outer membrane radius (r_2). For the set-up with a concentric, almost deaerated air gap as used in our study, both the experimental and the predicted fluxes do not increase with decreasing air gap. Because calculations show that the air gap resistance to mass transfer is about 30% of the total resistance at 300 mbar, see Fig. 10, one might expect that the flux increases with decreasing air gap. That this is not the case is caused by the fact that not only the air gap becomes smaller with decreasing condenser radius, but also the condenser surface. Model calculations for series F show that the temperature difference between condenser surface and cold water bulk changes from 0.4 to 1.6 °C with decreasing air gap from 2.7 to 0.06 mm. If the condenser surface had remained constant the flux would have increased by 20%.

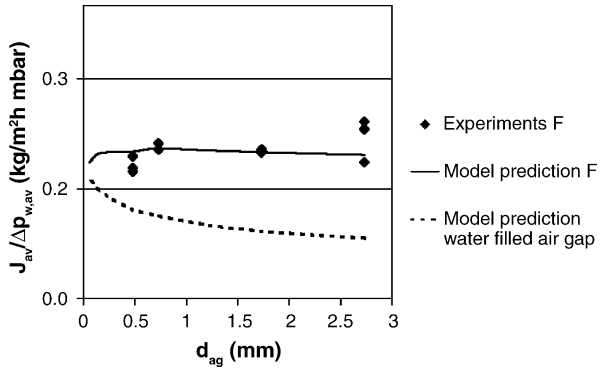

Fig. 13. Measured and calculated flux per driving force as a function of air gap width, series F ($T_{h,in}$ = 65 °C, ΔT_{top} = 10 °C, P_{ag} = 300 mbar).

Thus, reduction of a deaerated air gap can give some increase of the flux per driving force. However, reduction of the air gap has a considerable negative influence on the energy efficiency of the process, see Fig. 14. The model predicts a clear decrease in energy efficiency if the air gap becomes smaller than 0.2 mm. At this point the air gap loses much of its thermal insulation capacity. Although the experimental energy data points are quite scattered, they demonstrate a much larger decrease in energy efficiency with decreasing air gap. The most likely cause for this larger decrease in energy efficiency are product water droplets forming a bridge between the membrane fibre and the condenser surface. Calculations for the most extreme situation of a completely water filled air gap, which resembles direct contact MD, show that a water filled air gap reduces the theoretical energy efficiency from above 95% to about 76% (at 65 °C), see Fig. 14. Fig. 13 shows that a completely water filled air gap leads towards considerably lower water vapour fluxes than actually measured. This means that the air gap is not completely filled with product water. However, water bridges that are more likely to form in a smaller air gap, can explain the surprisingly high decrease in energy efficiency observed for smaller air gaps.

To support this theory most variable air gap measurements have been carried out with a cold water mass flow rate equal to that of the hot water so that its energy uptake can be mea-

Table 4
Energy loss and uptake of the cold water flow during measurement series F

d_{ag} (mm)	$\Delta E_{c,no\ \Delta T}$ (W)	$\Delta E_{c,no\ \Delta T}/A_{module}$ (W/m^2)	ΔE_c (W)	$\Delta E_{c,corr}$ (W)	E_{evap} (W)	$\Delta E_{c,corr}/E_{evap}$
2.7	−1.6	−132	3.0	4.6	4.9	0.95
1.7	−1.4	−134	2.4	3.8	4.0	0.95
1.7	−1.4	−139	2.7	4.2	3.7	1.11
0.7	−1.1	−138	3.3	4.5	3.8	1.19
0.7	−1.2	−147	3.2	4.4	3.7	1.19
0.45	−0.9	−137	3.1	4.1	3.3	1.21
0.45	−0.9	−130	3.0	3.9	3.2	1.21

sured. During these measurements the temperature of the hot water flow was first set at 55.0 °C, equal to that of the cold water flow. Under these conditions temperature decrease of the cold water flow was measured for some time to determine heat losses of the cold water flow to the surroundings ($\Delta E_{c,no\ \Delta T}$), see Table 4. The decrease in heat loss with decreasing air gap can be explained by the fact that the outer module radius also decreases with decreasing air gap, resulting in a smaller outer module surface. The ratio between heat loss and module surface is about constant. Next, the hot water flow temperature was set to 65.0 °C to start a 'normal' experiment. The energy change of the cold water flow in this experiment (ΔE_c) is also listed in Table 4. However, since the heat loss to the surroundings also takes place during this experiment, the energy transfer from the hot water flow to the cold water flow ($\Delta E_{c,corr}$) equals the measured energy change (ΔE_c) plus the heat loss ($\Delta E_{c,no\ \Delta T}$).

The intention of this membrane distillation process is that the cold water flow is heated by the latent heat of the product water (E_{evap}), which is therefore also listed in Table 4. This table shows that E_{evap} decreases with decreasing air gap. This is due to the decreasing energy efficiency, see Fig. 14, that results in a lower average driving force $\Delta p_{w,av}$. Fig. 15 shows clearly that $\Delta E_{c,corr}$ increases with respect to E_{evap} with decreasing air gap. At very small air gap $\Delta E_{c,corr}$ is even larger than E_{evap}, which means that the cold water flow is heated by other means than latent heat alone. The only way additional heat can be transferred from hot to cold flow, is by heat conduction. Calculations indicate that this amount of heat conduction is too large to take place through the vapour phase alone, but requires 10–15 vol.% of product water bridges between membrane fibre and condenser surface. Therefore, it must be concluded that a reasonably wide air gap of about 3 mm is preferred so that its heat insulating function cannot be destroyed by water bridges between membrane and condenser surface. Of course it is very important to remove all non-condensable gases from the air gap when a wide air gap is used, in order to minimise its resistance to mass transfer.

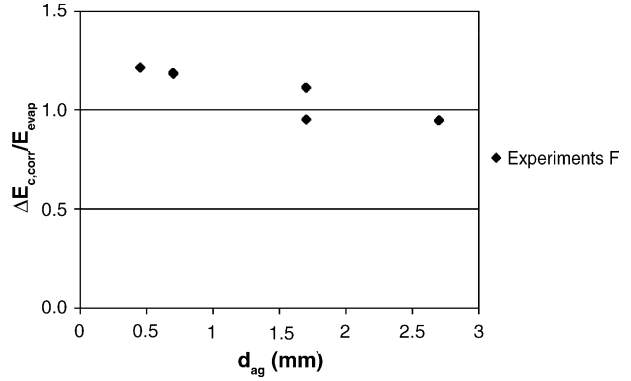

Fig. 15. Ratio between the corrected energy increase of the cold water flow ($\Delta E_{c,corr}$) and the latent heat of evaporation contained by the product water flow (E_{evap}) for variable air gap widths.

4. Conclusions

Counter current flow AGMD experimental results prove that the developed predictive model using membrane parameters determined from gas permeation experiments correctly describes the dependence of water vapour flux on all process variables. The thinnest hollow fibre membrane PE FA16 generated the highest fluxes, although it had a less permeable structure than the UPE test hollow fibre membrane. However, pressure drop and operability considerations make the PE VA12 hollow fibre membrane, with a diameter and wall thickness between those of the two above membranes, the preferred membrane. Reduction of the air gap total pressure from atmospheric to the saturated water vapour pressure of the hot water flow entering the membrane fibre raises the flux by a factor of 2.5–3. The measured energy efficiencies in this study (typically 85–90%) approach the theoretical values (95–98%) for AGMD, provided that the air gap is large enough, about 3 mm, to prevent product water forming bridges between membrane and condenser.

Acknowledgement

This research was founded by the Centre of Separation Technology, a cooperation of TNO-MEP and the University of Twente.

References

[1] S.T. Hsu, K.T. Cheng, J.S. Chiou, Seawater desalination by direct contact membrane distillation, Desalination 143 (2002) 279–287.
[2] L. Martínez, F.J. Florido-Díaz, Desalination of brines by membrane distillation, Desalination 137 (2001) 267–273.

[3] M. Gryta, M. Thomaszewska, J. Grzechulska, A.W. Morawski, Membrane distillation of NaCl solution containing natural organic matter, J. Membr. Sci. (2001) 279–287.
[4] K. Ohta, K. Kikuchi, I. Hayano, T. Okabe, T. Goto, S. Kimura, H. Ohya, Experiments on sea water desalination by membrane distillation, Desalination 78 (1990) 177–185.
[5] S. Kubota, K. Ohta, I. Hayano, M. Hirai, K. Kikuchi, Y. Murayama, Experiments on seawater desalination by membrane distillation, Desalination 69 (1988) 19–26.
[6] F.W. Banat, J. Simandl, Desalination by membrane distillation: a parametric study, Sep. Sci. Technol. 33 (2) (1998) 201–226.
[7] I.B. Elkina, P.P. Zolotarev, V.N. Nikulin, V.V. Ugrozov, R.Kh. Khamizov, Separation and concentration of salt solutions by membrane distillation with a gas slit, Colloid J. 57 (3) (1995) 299–302.
[8] D. Wirth, C. Cabassud, Water desalination using membrane distillation: comparison between inside/out and outside/in permeation, Desalination 147 (2002) 139–145.
[9] F. Banat, F.A. Al-Rub, K. Bani-Melhem, Desalination by vacuum membrane distillation: sensitivity analysis, Sep. Purif. Technol. 22 (2003) 75–87.
[10] M.C. García-Payo, M.A. Izquierdo-Gil, C. Fernández-Pineda, Air gap membrane distillation of aqueous alcohol solutions, J. Membr. Sci. 169 (2000) 61–80.
[11] C. Zhu, G.L. Liu, C.S. Cheung, C.W. Leung, Z.C. Zhu, Ultrasonic stimulation on enhancement of air gap membrane distillation, J. Membr. Sci. 161 (1999) 85–93.
[12] G.L. Liu, C. Zhu, C.S. Cheung, C.W. Leung, Theoretical and experimental studies on air gap membrane distillation, Heat Mass Transfer 34 (1998) 329–335.
[13] F.W. Banat, J. Simandl, Theoretical and experimental study in membrane distillation, Desalination 95 (1994) 39–52.
[14] M.A. Izquierdo-Gil, M.C. García-Payo, C. Fernández-Pineda, Air gap membrane distillation of sucrose aqueous solutions, J. Membr. Sci. 155 (1999) 291–307.
[15] F.W. Banat, J. Simandl, Membrane distillation for dilute ethanol separation from aqueous streams, J. Membr. Sci. 163 (1999) 333–348.
[16] C. Gostoli, G.C. Sarti, S. Matulli, Low temperature distillation through hydrophobic membranes, Sep. Sci. Technol. 22 (2 and 3) (1987) 855–872.
[17] R.W. Schofield, A.G. Fane, C.J.D. Fell, Heat and mass transfer in membrane distillation, J. Membr. Sci. 33 (1987) 299–313.
[18] L. Martínez-Díez, M.I. Vázquez-González, F.J. Florido-Díaz, Study of membrane distillation using channel spacers, J. Membr. Sci. 144 (1998) 45–56.
[19] C.M. Guijt, G.W. Meindersma, T. Reith, A.B de Haan, Air gap membrane distillation 1. modelling and mass transport properties for hollow fibre membranes, Sep. Purif. Technol. 43 (2005) 233–244.
[20] A.-S. Jönsson, R. Wimmerstedt, A.-C. Harrysson, Membrane distillation—a theoretic study of evaporation through microporous membranes, Desalination 56 (1985) 237–249.
[21] A.G. Fane, R.W. Schofield, C.J.D. Fell, The efficient use of energy in membrane distillation, Desalination 64 (1987) 231–243.
[22] C.M. Guijt, Influence of membrane properties and air gap on the performance of a membrane distillation module. Thesis, University of Twente, C.M. Guijt, Enschede, 2003.